Engineering Structures 117 (2016) 130–144

Contents lists available at ScienceDirect

Engineering Structures

journal homepage: www.elsevier.com/locate/engstruct

Behavior of stud connections between concrete slabs and steel girders under transverse bending moment

Zhaofei Lin [a,b], Yuqing Liu [a,*], Charles W. Roeder [b]

[a] Department of Bridge Engineering, Tongji University, Shanghai 200092, China
[b] Department of Civil and Environmental Engineering, University of Washington, Seattle, WA 98195-2700, USA

ARTICLE INFO

Article history:
Received 27 May 2015
Revised 6 March 2016
Accepted 7 March 2016

Keywords:
Steel–concrete composite bridges
Stud connections
Transverse bending moment
Model tests
Numerical simulations

ABSTRACT

The effect of transverse bending moment on stud connections is usually ignored in the design of steel–concrete composite bridges due to beam web flexibility. However, large transverse moment may arise near transverse stiffeners and diaphragms, because they constrain and stiffen the webs and cause tensile forces in stud connectors. Large web spacing and wide cantilevers increase these effects. This study experimentally and numerically investigates this behavior. Four groups of pull-out tests of a single stud connector under tension force are performed, and they provide insight into the behavior of stud connectors under direct tensile loading. Then four stud connections at interfaces near transverse stiffeners are tested to investigate their behavior under transverse bending moment. Numerical models of the stud connections are established to explore local behavior. The pull-out tests show that stud height greatly influences failure mode, tension strength and ultimate separation between the steel flange and the concrete slab. A tension–separation relationship is developed from the test results and used in subsequent numerical simulations. The stud connection tests suggest that longer studs can increase the bending moment and deformation capacities. Reduced longitudinal stud spacing significantly increases the stiffness, but may result in brittle failure of the concrete slab. Stud connectors should not be welded immediately over transverse stiffeners. Numerical simulations and test data compare well, and numerical results predict tensile forces in studs located near the steel web and in the region near stiffeners and other web restraint. The stud connectors in the two innermost rows on either side of a transverse stiffener provide the restraint to develop the tensile force in the studs caused by transverse bending moments. The force in a stud increases as its distance from the steel web increases and its distance from the transverse stiffener decreases. Shear–tension interaction should be checked for these connectors. Details of transverse stud arrangements with various stud heights are provided.

1. Introduction

Steel–concrete composite girders are extensively used in bridge construction due to their light weight, large load capacity and relatively shallow girder depth. Headed stud connectors are usually welded to the top flange of the steel girder and embedded into the concrete slab to develop the composite action [1,2]. The studs resist the horizontal and vertical relative movements between the steel flange and the concrete slab [3,4]. Thus, the studs will resist both the horizontal shear force and any tensile force that develops.

Extensive studies [5–14] on the behavior of the stud connections between concrete slabs and steel girder top flanges under shear force are described in the literature, but few studies evaluate the behavior of stud connections under transverse bending moment at this interface. Xu et al. [15] performed biaxial load experiments on stud connectors using push-out tests, and showed that the bending-induced cracks in the slab adversely affect stud performance. Their research focused on the influence of the local transverse bending moment in the concrete slab on a single stud connector. The effect of transverse bending moment at the interface on stud connections is seldom investigated and usually ignored in the design of a composite bridge, because the high flexibility of steel webs limits any moment transfer between the slab and the girder flange. However, large bending moment transfer may arise near transverse stiffeners and diaphragms since the local stiffness is increased. The increased local stiffness may cause increased tensile stress in concrete slabs and tension force in stud connectors [16]. This may be further increased by composite girders with large web spacing and wide cantilevers in the concrete

* Corresponding author. Tel.: +86 21 65983116; fax: +86 21 65986507.
E-mail address: yql@tongji.edu.cn (Y. Liu).

http://dx.doi.org/10.1016/j.engstruct.2016.03.014
0141-0296/

Nomenclature

A_s	area of the shank of the headed stud
d	separation between steel beam and concrete block in pull-out tests
d_{cp}	separation at peak transverse support bending moment
d_s	diameter of the shank of a stud connector
d_p	separation at peak tension load in pull-out tests
d_u	separation at 90% of the peak tension load on the post-peak descending branch in pull-out tests
E_c	elastic modulus of concrete
E_s	elastic modulus of steel
f_c	cylinder compressive strength of concrete
$f_{c,cube}$	cube compressive strength of concrete
f_t	tensile strength of concrete
G_f	energy required to open a unit area of crack
f_u	tensile strength of headed stud material
f_{us}, f_{ur}	ultimate strength of structural steel and reinforcements, respectively
f_{ys}, f_{yr}	yield stress of structural steel and reinforcements, respectively
h_s	overall height of a stud connector
h_{ef}	effective embedment depth of a stud connector
k_c	bending stiffness of stud connection at the interface
k_s	shear stiffness of a stud connector
k_t	tension stiffness of a stud connector
M_u	applied maximum transverse support bending moment
n_l	number of stud connectors in the longitudinal direction
s_l	stud spacing in the longitudinal direction
T	tension force in a stud connector
T_u	tension strength of a stud connector
σ_u	ultimate strength of steel material
σ_y	yield stress of steel material
ε'_c	strain corresponding to the compressive strength of concrete
ω_c	failure cracking displacement

slab. The approach bridges of Shanghai Yangtze River Bridge in Shanghai, China, are steel–concrete composite bridges that illustrate this concern. Each composite bridge consists of two separate parallel composite box girders, each of which is comprised of a steel U-girder attached to a concrete slab through stud connectors. The details of the cross section at mid-span are shown in Fig. 1. The full width of the concrete deck slab is 17.15 m and is divided into three traffic lanes. The outmost traffic lane is reserved for light rail trains in the future. The web spacing and the width of each concrete cantilever are about 9.15 m and 4 m, respectively, which is very uncommon in existing composite bridges and is a great concern during the design. Web stiffeners are required at some locations, and significant stiffening of the web occurs at these locations. The stiffened web results in significant increases in the rotational stiffness of the flange and web, and increased local restraint to the slab at this local region. Hence, local moment transfer and significant tensile forces in the studs may occur in this region. Therefore, this research studies the behavior of stud connections between concrete slabs and steel girder top flanges under transverse bending moment located near transverse stiffeners.

In this paper, the static behavior of stud connections is investigated both experimentally and numerically. The experimental work consists of pull-out tests and concrete slab-to-steel girder top flange connection tests. Four groups of pull-out specimens are tested to study the behavior of a single stud as a function of stud height under direct tensile force. Then, four concrete slab-to-steel girder top flange connections are tested to investigate their global behavior under transverse bending moment at a stiffener.

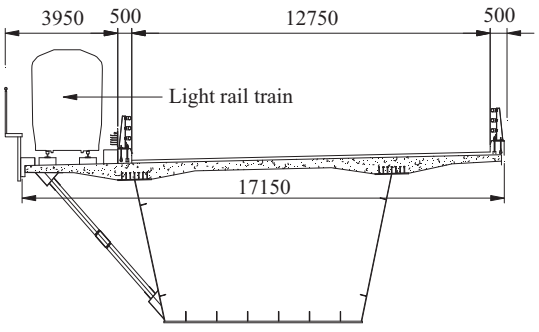

Fig. 1. Cross section at mid-span (mm).

The chosen variables are stud height, longitudinal stud spacing and stud location. Based on the pull-out test results, the effect of overall stud height on the tension stiffness, tension strength and ductility of a stud connector is evaluated. An expression relating tension to separation between the stud and beam flange is developed and used in subsequent numerical simulations. The global behavior of the four stud connections are analyzed with this analytical model, compared to experimental results, and then used to evaluate the effect of key parameters. Then, finite element models are established to derive the local behavior within these connection regions. Distribution of contact stress at the steel–concrete interface and distribution of tensile force in stud connectors are discussed in detail.

2. Pull-out tests

Tensile force arises in some stud connectors when a stud connection is subjected to transverse bending moment; thus, pull-out tests are carried out at first to study the behavior of a single stud connector under direct tensile force.

Four groups of three identical pull-out specimens, denoted as T1, T2, T3 and T4, respectively, were tested. Previous researches [17–19] have shown that stud height has a great influence on stud behavior under tensile force, and stud height is the primary variable for the pull-out tests. The overall stud height, h_s, is 100 mm, 200 mm, 300 mm and 400 mm for Groups T1, T2, T3 and T4, respectively. The stud shank diameter is 22 mm for all the specimens.

The details of the pull-out specimens are shown in Fig. 2. Each specimen consists of a steel beam, a concrete block and a single stud connector. The steel beam is designed with sufficient strength and stiffness to ensure it remains in the elastic range through the load needed for stud fracture or cone failure of the concrete. The concrete block is cast in the horizontal position, as is done for composite girders in practice. Bond stress at the steel–concrete interface is diminished by greasing the contact surface between the steel beam and the concrete block.

2.1. Material properties

Six 150 mm × 150 mm × 150 mm concrete cube specimens are cast at the same time as the concrete blocks for the pull-out test specimens to provide material properties of the concrete. The

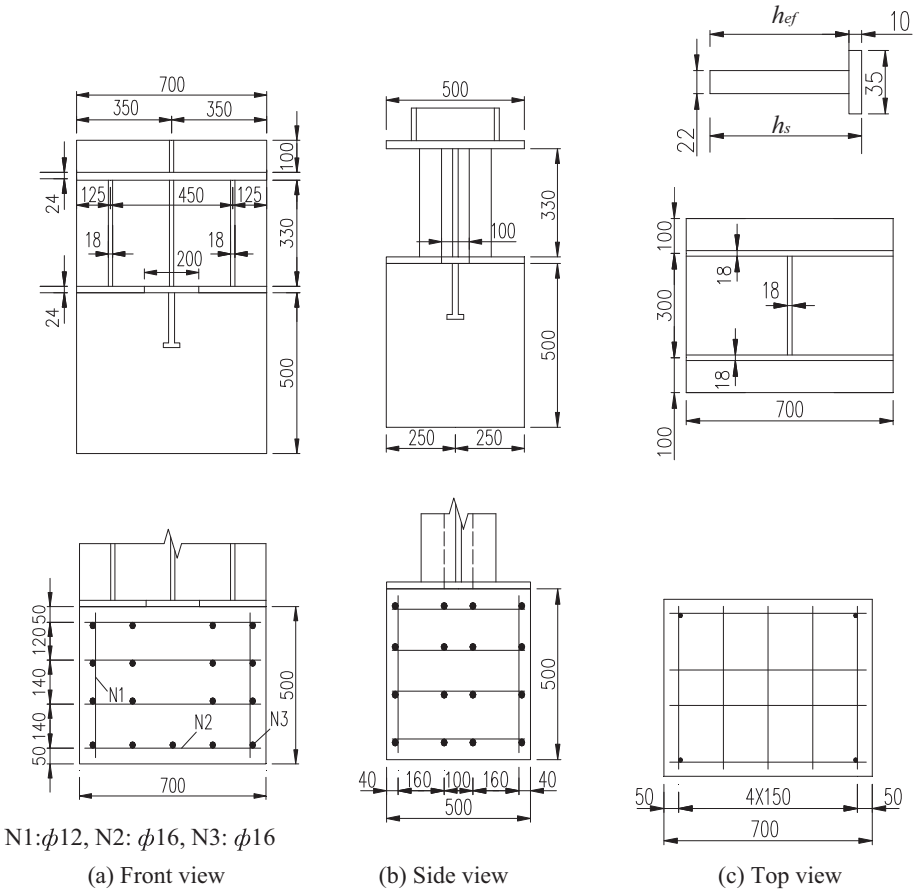

Fig. 2. Details of pull-out specimens (mm).

Table 1
Material properties of concrete.

Modulus of elasticity (E_c)	36.34	GPa
Nominal compressive strength	60.0	MPa
Average Compressive strength at 28 days ($f_{c,cube}$)	62.9	MPa

Table 2
Material properties of structural steel, rebar and headed stud.

Component	E_s (GPa)	σ_y (MPa)	σ_u (MPa)
Structural steel	206	437	565
Rebar	200	349	419
Headed stud	200	423	519

measured concrete strength is listed in Table 1. The modulus of elasticity is computed using the average compressive strength according to the specified equation in JTG D62-2004 [20]. The yield and ultimate strengths of structural steel, rebar and headed stud material are provided by the suppliers and are summarized in Table 2.

Fig. 3. Test set-up of pull-out tests.

2.2. Loading procedure and measurements

The test set-up is shown in Fig. 3. The specimens are tested using two identical hydraulic jacks with a capacity of 2000 kN. The jacks are placed symmetrically to ensure the stud is subject to uniaxial tension. First, force control is applied with a loading rate of 5 kN/min till 70% of the expected failure load. Then, displacement control is used with a loading rate of 0.5 mm/min. Four displacement sensors are symmetrically installed to measure the relative separation between the top surface of the concrete block and the bottom surface of the steel beam. The mean value of their readings is used in the description of the test results. All the specimens are loaded until failure is observed.

(a) steel side

(b) concrete side

Fig. 4. Concrete cone pull-out failure.

(a) steel side

(b) concrete side

Fig. 5. Stud failure.

2.3. Tests results

2.3.1. Failure modes

Two failure modes are observed during the tests: concrete cone pull-out failure (CF) and stud fracture (SF), as shown in Figs. 4 and 5. The three specimens of Group T1 with a height–diameter ratio of 4.55 failed due to cone pull-out failure. The other three groups with a minimum height–diameter ratio of 9.09 all failed due to stud shank fracture. The failure surface occurred at a small distance from the weld collar, and the necking phenomenon is clearly observed. This shows that stud height has a great effect on the failure mode as noted in prior research [17].

2.3.2. Strength and stiffness

The test results of tension strength, T_u, and stiffness, k_t, are summarized in Table 3. The average tension strength of Group T1 failed due to concrete cone pull-out is 108.7 kN. The average strengths of Groups T2, T3 and T4 failed due to stud fracture are 163.0 kN, 171.3 kN and 165.3 kN, respectively. The difference among the average strengths of the Groups T2, T3 and T4 is very small, which indicates that stud height has little influence on tension strength in the case of stud fracture failure. This also is consistent with prior research [17] that shows that fracture of studs with adequate embedment depth is controlled by tensile strength of the stud connector. The average strength of all specimens with fracture of the stud is 166.5 kN, which is about 1.53 times of the average strength of those failed due to concrete cone pullout. This tensile fracture resistance compares well with the tensile yield capacity (160.8 kN) of the studs based upon the properties of Table 2, but it is somewhat smaller than the ultimate tensile capacity (197.2 kN) suggesting that the fracture resistance is affected somewhat by the weld and heat affected zone of the shear stud.

Eqs. (1) and (2) are the design tensile strength formulas for steel failure and concrete cone pull-out failure, respectively, given in ACI 318-08 [21]. It can be noted that the tensile strength of stud material, f_{uta}, is used in Eq. (1) to calculate the tensile strength of stud connectors instead of the yield strength, f_{ya}. According to the commentary of ACI 318-08, the tensile strength of anchors is best represented as a function of f_{uta} rather than f_{ya} because the large majority of anchor materials do not exhibit a well-defined yield point. To achieve the same level of safety, the strength reduction factor for use with f_{uta} employs a lower value than that for use with f_{ya}. Therefore, the smaller experimental tensile strengths in comparison with the calculated ones would not be a concern in design, which will be proved by the subsequent comparison of the experimental tensile strengths with the design values predicted by ACI.

$$\phi N_{sa} = \phi A_{se} f_{uta} \tag{1}$$

where ϕ is the strength reduction factor and equals 0.75 and 0.7 for steel failure and cone pull-out failure, respectively, N_{sa} is the nominal steel strength and A_{se} is the cross-sectional area of a headed stud.

Table 3
Results of pull-out tests.

Groups	Test no.	T_u (kN)	k_t (kN/mm)		d_p (mm)	d_u (mm)	Failure mode
			Test	Eq. (1)			
ST1	1	111.8	212.4	844.3	3.56	3.89	CF
	2	98.7	170.4		1.13	1.36	CF
	3	115.5	363.0		1.94	2.78	CF
	Mean	**108.7**	**248.60**		**2.21**	**2.68**	–
ST2	1	154.6	276.1	400.0	10.17	15.18	SF
	2	174.8	179.3		10.86	18.52	SF
	3	159.6	225.6		10.36	16.88	SF
	Mean	**163.0**	**227.00**		**10.46**	**16.86**	–
ST3	1	168.8	192.7	262.0	12.57	16.56	SF
	2	172.2	215.7		13.38	17.81	SF
	3	172.8	193.6		13.54	20.20	SF
	Mean	**171.3**	**200.67**		**13.16**	**18.19**	–
ST4	1	171.9	195.2	194.8	18.97	24.80	SF
	2	159.3	281.3		16.48	19.66	SF
	3	164.6	175.0		11.97	17.02	SF
	Mean	**165.3**	**217.17**		**15.81**	**20.49**	–

$$\phi N_{cb} = \phi 10 \frac{A_{Nc}}{A_{Nc0}} \psi_{ed,N} \psi_{c,N} (h_{ef})^{1.5} \sqrt{f'_c} \quad (2)$$

where N_{cb} is the nominal concrete cone pull-out strength, A_{Nc} and A_{Nc0} are the projected concrete failure area and the projected concrete failure area with an edge distance equal to or greater than 1.5 h_{ef}, respectively. $\psi_{ed,N}$ is the modification factor for edge effects, $\psi_{c,N}$ is modification factor accounting for the effects of cracking in concrete, h_{ef} is the effective embedment depth of a stud connector and f'_c is the specified compressive strength of concrete.

The experimental tensile strengths are compared with the design and nominal strengths predicted by Eq. (1) or (2), as shown in Fig. 6. The nominal strength of stud material is 400 MPa. The ratios of the design strength to the average value of the measured strengths are 0.48, 0.70, 0.67 and 0.69 for Groups T1, T2, T3 and T4, respectively. The ratios increase to 0.68, 0.93, 0.89 and 0.92, respectively, when ϕ = 1.0. ACI 318-08 gives conservative predictions for both concrete cone pull-out failure and steel failure.

Tension stiffness is needed to perform elastic analysis of composite structures with stud connectors. Few studies on tension stiffness of studs are available in the literature. There are two direct methods to address this issue. The first is to ignore the friction and bond between concrete and stud shank and approximate the stiffness based upon uniaxial deformation of the stud shank as shown in Eq. (3).

$$k_t = E_s A_s / h_{ef} \quad (3)$$

The second is to neglect the relative separation between steel element and concrete element and regard the tension stiffness as infinity. The separation between the steel flange and the concrete block is measured during the pull out tests, and the accuracy of the first method is checked based on test results. The tested tension–separation curves are plotted in Fig. 6. The curves of all the specimens that failed due to stud shank fracture are almost linear until at least $0.5T_u$. Similar behavior can also be noted for specimens with cone pull-out failure. Thus, the experimental tension stiffness, k_t, is defined as the secant modulus of the point whose corresponding applied tension load is $0.5T_u$ on the tension–separation curve. Table 3 shows the tension stiffness derived from the tests and predicted using Eq. (3), and the stiffness predicted by Eq. (3) does not agree well with the experimental stiffness. The experimental stiffness of the four groups have considerable scatter. The stud height clearly has little influence on the tension stiffness. In contrast, stud height has a great influence on tension stiffness according to Eq. (3). With decreasing stud height, the stiffness predicted using Eq. (3) increases significantly. Therefore, it can be concluded that Eq. (3) does not provide a reasonable prediction of tension stiffness, and an improved model is needed.

2.3.3. Peak and ultimate separation between steel and concrete

The separation at the maximum tension load is defined as peak separation, d_p. The separation at 90% of the maximum tension load in the descending branch of tension–separation curve is defined as ultimate separation, d_u, which provides a measure of the ductility of stud connectors. Both the average peak and ultimate separations of Group T1 are much smaller than those of the other three groups, as shown in Table 3. Taking Group T2 as an example, the average peak and ultimate separations are about 4.7 and 6.3 times larger than those of Group T1, respectively. For specimens with tensile failure of the stud, both the average peak and ultimate separations increase as the stud height increases. This suggests that a long stud connector develops larger separation between the steel and the concrete than a shorter stud connector at the same tensile force.

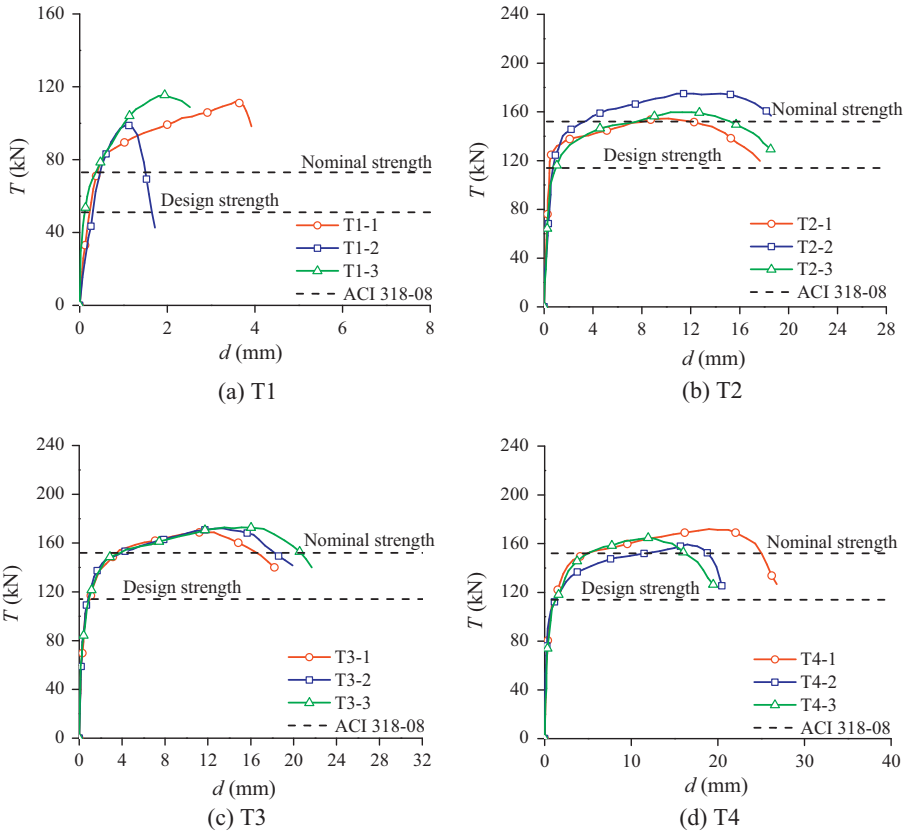

Fig. 6. Tension–separation curves of pull-out tests.

2.3.4. Tension–separation relation

The tension–separation curve of stud connectors is needed to theoretically evaluate the tensile force in stud connectors subjected to transverse bending moment. To derive the expression of tension–separation relation, all the tested curves of the specimens failed due to stud fracture are non-dimensionalized using the measured tension strengths and peak separations, as shown in Fig. 7. The non-dimensionalized curves are very similar except for one curve. Thus, an expression of non-dimensionalized load–separation relation is derived by curve fitting to these data. For the resulting curve, the tension force in a stud connector reaches the maximum value at the peak separation, and the resulting curve is defined in Eq. (4).

$$\frac{T}{T_u} = \frac{4}{3}\left(\frac{d}{d_p}\right)^{1/4} - \frac{1}{3}\left(\frac{d}{d_p}\right) \tag{4}$$

To derive the expression of dimensional tension–separation curves, the formulas of estimating tensile strength and peak separation are necessary. Tension strength can be calculated using Eq. (1) with $\phi = 1.0$. As discussed in Section 2.3.2, Eq. (1) gives somewhat conservative predictions if the nominal material properties are used but overestimates the tensile strength if the measured material properties are used. If the tensile strength is computed using the measured material properties, Eq. (4) would overestimate the tensile force resisted by a stud connector at a particular separation and thus overestimate the stiffness and moment capacity of stud connections. Therefore, nominal material properties are suggested to be used in Eq. (1) if experimental tensile strengths from pull-out tests are not available.

The formula of peak separation is derived by fitting the tested data of this work as a function of effective embedment depth, h_{ef}, as shown in Eq. (5) and Fig. 8.

$$d_p = 0.027h_{ef} + 5.4 \tag{5}$$

3. Concrete slab-to-steel girder top flange connection tests

Groups of stud connectors welded to a steel flange attached to a web with transverse stiffeners and embedded into a concrete slab are tested under transverse support bending moment in a second series of tests. The behavior of stud-to-flange connections is expected to be very different at locations where the flange is stiffened by web stiffeners, because these locations attract larger transverse bending moments to the weld group. Hence, evaluation of these local effects is a major focus of these stud group tests.

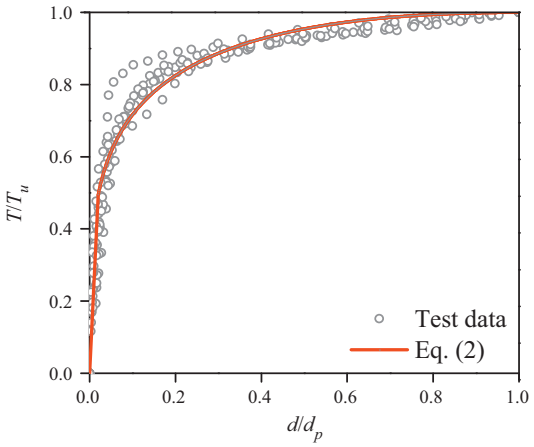

Fig. 7. Non-dimensionalized tension–separation relation.

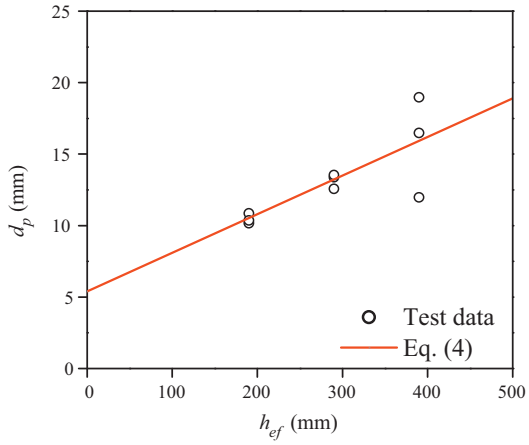

Fig. 8. Peak separation.

3.1. Test specimens

Four specimens, denoted as M1, M2, M3 and M4, respectively, are fabricated and tested. The details of specimen M1 are shown in Figs. 9 and 10. The other three specimens are the same as specimen M1, except that the arrangement of stud connectors is different. The chosen variables are stud height, stud location and longitudinal stud spacing, as shown in Fig. 11. Each specimen consists of a steel cantilever beam, a steel web with transverse stiffeners attached to a steel top flange and a reinforced concrete slab, as shown in Figs. 12 and 13. The cantilever beam is designed to facilitate application of the load and is bolted to the steel web and transverse stiffeners using high strength bolts. A group of stud connectors are welded to the steel flange and embedded into the concrete slab to connect them together. The stud diameter is 22 mm for all the specimens.

For specimen M1, the overall stud height is 200 mm. The longitudinal stud spacing is 300 mm. The studs are symmetrically arranged on the two sides of the transverse stiffener without any stud located at the same longitudinal location as the transverse stiffener, as shown in Fig. 11. For specimen M2, the stud arrangement is the same as M1 but the stud height is 300 mm. For specimen M3, one row of the stud connectors is located over the transverse stiffener. For specimen M4, the longitudinal stud spacing is 150 mm, and the stud rows straddle the stiffener as with specimens M1 and M2. The stud height for M3 and M4 is 200 mm. Bond stress and friction at the steel–concrete interface are reduced by greasing the top flange of the steel beam for all specimens.

3.2. Material properties

The material properties of steel beams, reinforcements and stud connectors are the same as those for the pull-out tests and are given in Table 2. Although the concrete material is also the same as the pull-out specimens, the material tests of this part yields a slightly higher value of 65.9 MPa at 28 days.

3.3. Loading procedure and measurements

To facilitate the application of load, the specimens are placed under a self-reaction frame. The concrete slab is anchored to the strong floor using four prestressed anchors. A hydraulic jack is installed between the reaction frame and the cantilever beam to apply the transverse bending moment. Force control is used during the whole test. The distance from the loading point to the centerline

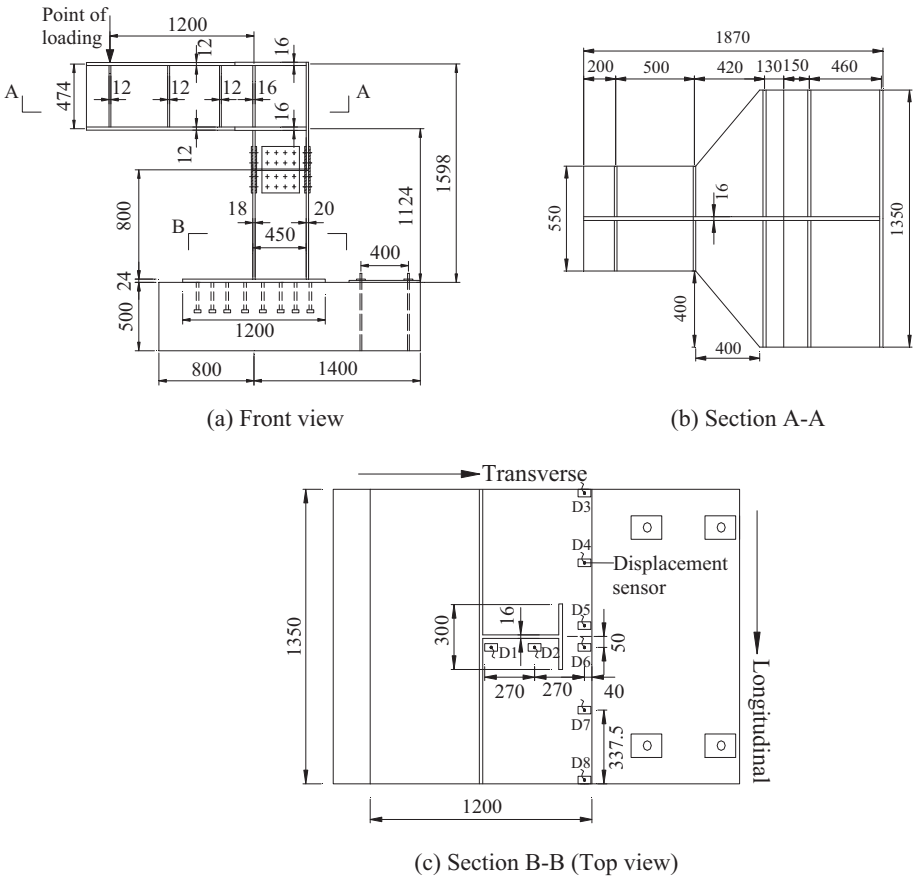

Fig. 9. Details of concrete slab-to-steel girder top flange connection specimens (mm).

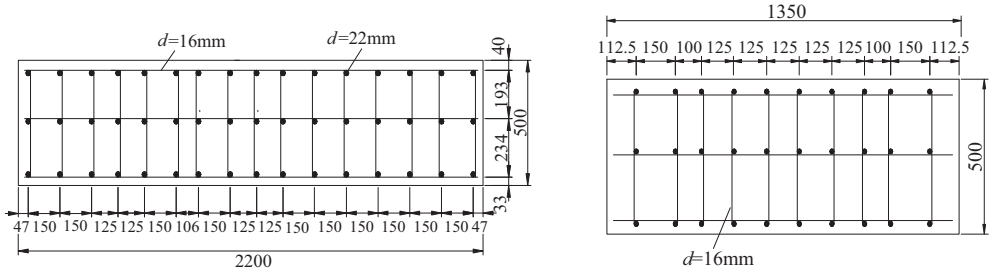

Fig. 10. Details of reinforcements in concrete slab (mm).

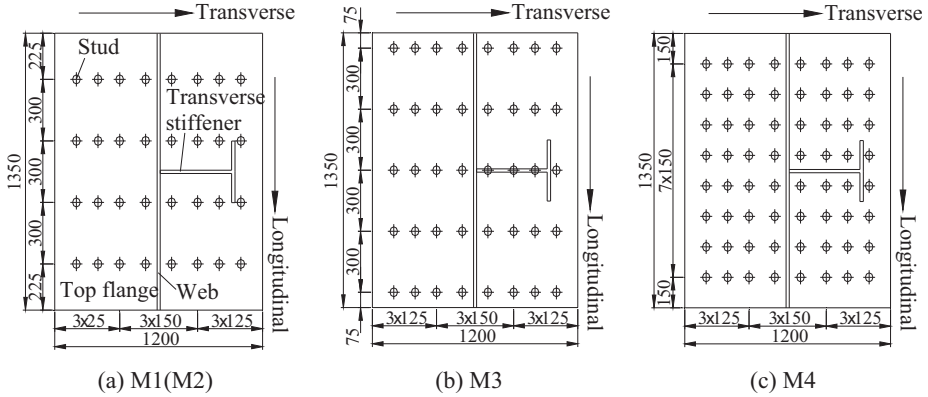

Fig. 11. Arrangement of stud connectors (mm).

Fig. 12. Test set-up of stud connection tests.

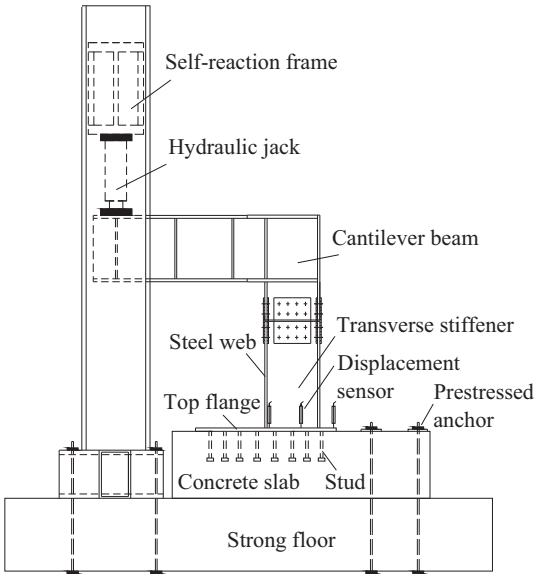

Fig. 13. Schematic of test set-up of stud connection tests.

of the steel web is 1200 mm. The specimens are monotonically loaded until the maximum load is reached. Eight displacement sensors, denoted as D1–D8, are installed near the transverse stiffener and one edge of the top flange to measure the relative separation between the steel flange and the concrete slab, as shown in Fig. 9(c).

3.4. Test results

3.4.1. Failure modes

The tests are performed under force control and the specimens are not tested to failure. The separation between the top flange and the concrete slab can be obviously observed, which clearly indicates that some stud connectors develop a lot of plastic deformation under tension force, as shown in Fig. 14(a). The concrete is removed after completion of the test to evaluate the condition of the studs. No stud fracture is noted, as shown in Fig. 14(b). All the concrete slabs are intact and no cracking is observed on the outside surfaces.

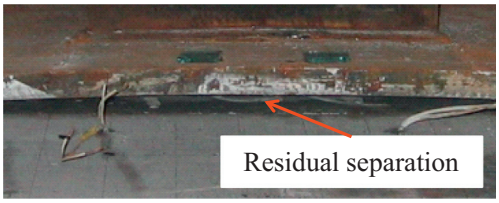

(a) Residual separation at the interface (M2)

(b) Stud connectors (M2)

Fig. 14. Failure mode.

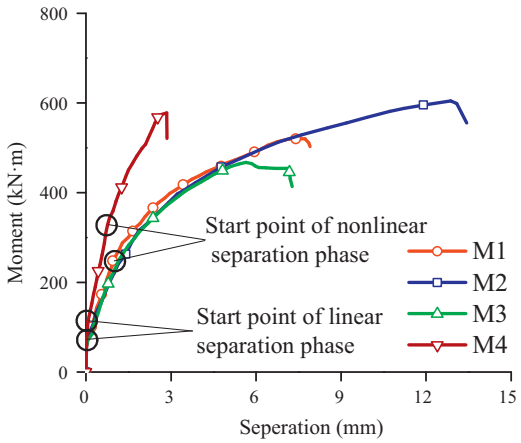

Fig. 15. Moment–separation curves of the stud connection tests.

3.4.2. Moment–separation curves

Fig. 15 presents the moment–separation curves measured during the connection tests. The moment is computed by multiplying the applied load by the distance from the loading point to the centerline of the steel web. The separation is the mean value of the readings of displacement sensors D5 and D6. Note that the ascending branch of each specimen consists of three phases. The first phase has no separation between steel and concrete. Virtually no separation occurs before the moment reaches about 70 kN m for specimens M1, M2 and M3, while that moment is about 120 kN m for specimen M4. This may be caused by the friction and bond stress at the interface between the stud shank and concrete slab, since the tension–separation curves of the pull-out tests of the studs present the identical behavior. In the second phase, separation increases linearly with moment until the moment reaches approximately 240 kN m for specimens M1, M2 and M3 and 320 kN m for specimen M4. The third phase has nonlinear separation behavior with more rapidly increasing separation with increasing moment until the maximum moment is attained.

The stiffness of the concrete slab-to-steel girder top flange connection, k_c, is defined as the secant modulus at the end point of the linear separation phase in this study. Table 4 lists the stiffness

Table 4
Results of stud connection tests.

Specimen	n_l	s_l (mm)	h_s (mm)	M_u (kN m)		$M_{u,FEM}/M_{u,test}$	k_c (kN m/mm)		$k_{c,FEM}/k_{c,test}$	d_{cp} (mm)
				Test	FEM		Test	FEM		
M1	4	300	200	520.2	540.1	1.04	215.9	170.1	0.79	7.20
M2	4	300	300	604.4	652.6	1.08	172.4	151.2	0.88	12.83
M3	5	300	200	467.4	473.4	1.01	191.2	152.0	0.79	5.61
M4	8	150	200	577.6	571.0	0.99	417.5	428.8	1.03	2.82

computed from the test data. The stiffness of specimen M2 is about 20% smaller than that of specimen M1, and this may be explained by the observation that the stiffness of a 300 mm stud is a little smaller than that of a 200 mm stud in the pull-out tests. Specimen M3 had one row studs located immediately over the transverse stiffener and its stiffness is about 11% smaller than that of specimen M1. In contrast, specimen M4 has 150 mm longitudinal stud spacing and it has 93% larger stiffness than specimen M1. This comparison suggests that the stiffness is very sensitive to longitudinal stud spacing.

3.4.3. Moment capacity and peak separation

The moment capacity, M_u, and the peak separation, d_{cp}, for each specimen are listed in Table 4. The moment capacity of specimen M1 is 520.2 kN m. Specimen M2 with the 300 mm studs and specimen M4 with the stud spacing of 150 mm have approximately 16.2% and 11.0% increases in moment, respectively. For Specimen M3 with one row of stud connectors locates at the same longitudinal location as the transverse stiffener, the moment capacity is 10.0% smaller than specimen M1. However, it should be emphasized that none of these specimens are tested to failure. The test is continued until the moment reaches its peak value, and the test is continued shortly thereafter.

Since force control is used during the whole test period, the descending branches of the moment–separation curves are not available from the test data. Thus, the peak separation instead of the ultimate separation is used to assess the deformation capacity of these specimens. The peak separation of specimen M1 is 7.20 mm. Specimen M2 has approximately 78.2% larger peak separation than specimen 1, and specimens M3 and M4 have approximately 22.1% and 60.8% smaller peak separation than M1, respectively. The peak separation of specimen M4 is only 2.82 mm. In order to find the reason of the sudden reduction in moment capacity at the relatively small separation, the concrete slab in specimen M4 is removed after the test to examine the condition of the stud connectors, and no stud fracture is observed. Further, no cracking and crushing are noted on the outside surfaces of the concrete slab. Thus, the reason for the sudden decrease in resistance is unclear, and it is also uncertain as to whether strength would be gained with significant increases in separation. This suggests that it is preferable to use long stud connectors in the region near transverse stiffeners, since long studs can increase both the moment and deformation capacities. Stud connectors should not be installed at the same longitudinal location as transverse stiffeners, because both moment capacity and peak separation are reduced. In addition, dense arrangement of stud connectors increases the bending stiffness of stud connections but may result in significant reduction in resistance at smaller separation. Therefore, careful attention should be paid when dense arrangement is required.

4. Numerical Modeling on concrete slab-to-steel girder top flange connections

The global behavior of the four stud connections has been obtained from the experimental work; however, the local behavior in the connection region is still unclear due to the difficulty in measuring them. Therefore, detailed numerical models are developed using the general finite element program ABAQUS [22] to explore the local behavior as shown in Fig. 16. To save computational time, one half of each specimen is molded because of its symmetry in longitudinal direction. In the finite element models, all the components, including the concrete slab, steel girder, reinforcements and stud connectors, are simulated. Material and geometric nonlinearity are also considered.

4.1. Element type and mesh

The solid element C3D8R is used to simulate the concrete slab and the steel girder, while the reinforcing steel is modeled with the truss element, T3D2. The stud connectors are simulated using the CARTESIAN connector element, which provides a connection between two nodes that allows independent behavior in three local Cartesian directions. The force in each direction depends on the relative displacement between the two nodes in that direction. Both linear and nonlinear behavior can be defined for this connection type. In the model, one node is created at the center of the top surface of stud head, while another node is located at the center of the interface between the stud shank and top flange.

A mesh refinement study is completed, because the top flange is subjected to the out of plane bending moment caused by the stud, and mesh size in the thickness direction of the top flange has a great influence on the behavior. Five elements with an element size of 4.8 mm are used in the thickness direction, because a finer mesh has little influence on the predicted behavior. A coarser mesh is applied in other less critical regions to save computational time.

4.2. Interaction

Contact elements are employed at the interface between the concrete slab and steel girder top flange. Hard contact and a penalty frictional formulation are used to simulate the normal and tangential behavior, respectively. The coefficient of friction is taken as 0.4 as recommended from the experimental studies of Cook and Klingner [23]. The embedded constraint is applied to the reinforcing elements and the concrete elements. Perfect bond between reinforcement and surrounding concrete is assumed.

4.3. Loading and boundary conditions

Symmetric boundary conditions are applied to the longitudinal symmetry plane. The three translational movements at the bottom surface of the concrete slab are restrained. The translational movement of the anchorage area at its top surface is also constrained. A vertical displacement is applied at the loading area to apply the bending moment.

4.4. Material modeling

The stress–strain curve proposed by Carreira and Chu [24], as shown in Fig. 17(a) and Eq. (6), is employed to simulate the concrete compressive behavior.

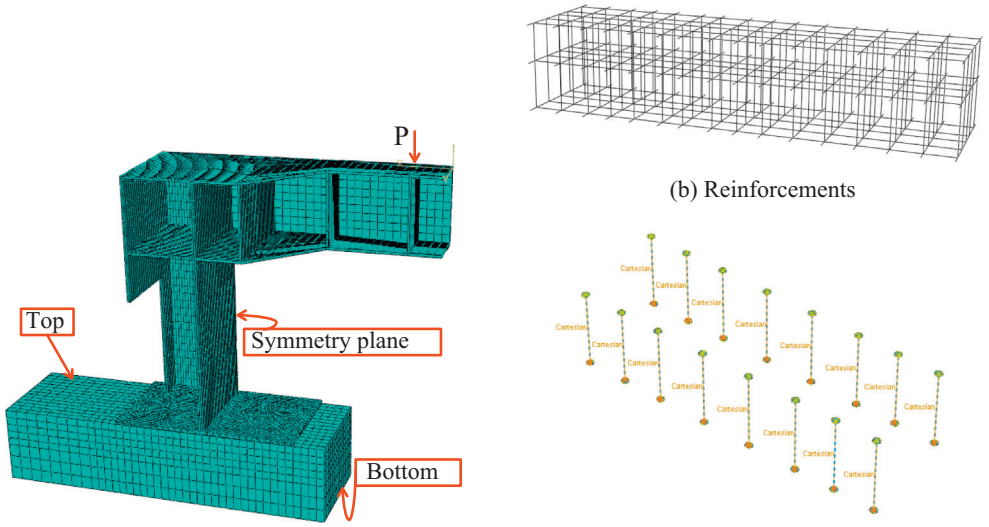

(a) Meshed model (b) Reinforcements (c) Stud connectors (M1)

Fig. 16. The finite element model.

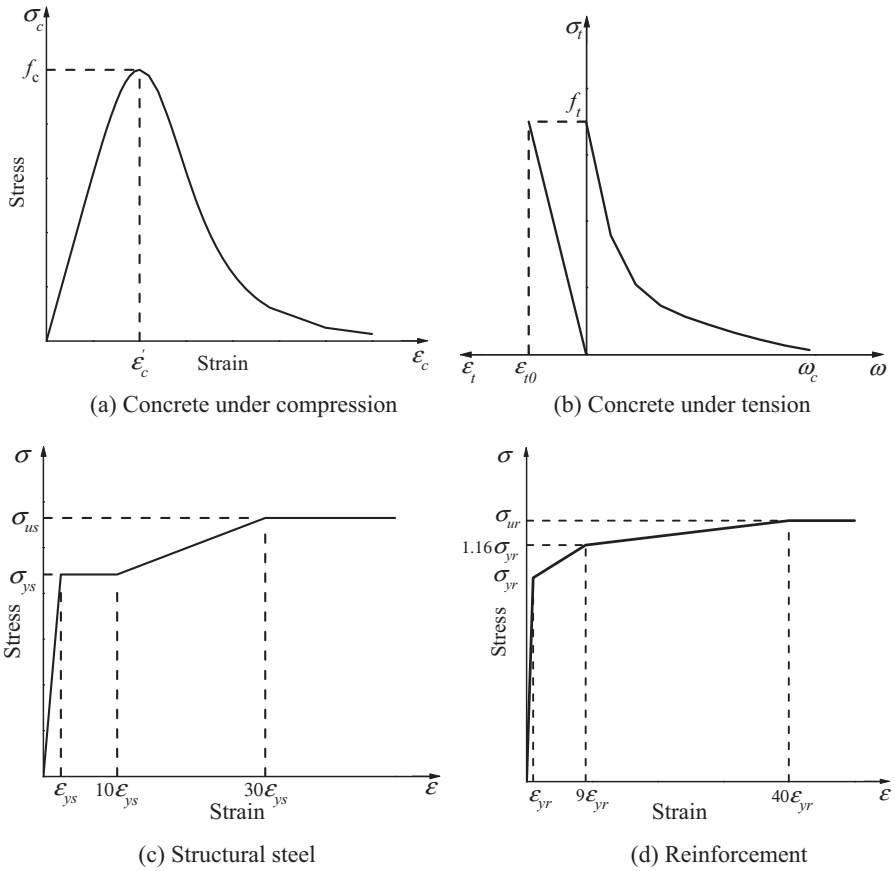

(a) Concrete under compression (b) Concrete under tension

(c) Structural steel (d) Reinforcement

Fig. 17. Constitutive law of steel and concrete materials.

$$\sigma_c = \frac{f_c \gamma(\varepsilon_c/\varepsilon_c')}{\gamma - 1 + (\varepsilon_c/\varepsilon_c')^{\gamma}} \tag{6}$$

where σ_c = compressive stress, f_c = the cylinder compressive strength of concrete, ε_c = compressive strain, ε'_c = strain corresponding to the compressive strength; and $\gamma = (f_c/32.4)^3 + 1.55$, $\varepsilon'_c = 0.002$.

The stress–strain relationship is assumed to be linear up to 40% of the compressive strength.

The tensile stress, σ_t, used in the material model increases linearly until the ultimate tensile stress, f_t, is developed, where f_t is computed based on the compressive strength using the ACI 318-08 equation [20]. The stress–displacement relationship

proposed by Cornelissen et al. [25] is used to simulate deformations after initiation of cracking as shown in Fig. 17(b) and Eqs. (7) and (8). G_f is the energy required to open a unit area of crack using brittle fracture concepts and is calculated using Eq. (9) [26]. A stress–displacement relationship is used to simulate the post-failure behavior, because the stress–strain relationship may introduces unreasonable mesh sensitivity into the results if significant regions of the model are inadequately reinforced [19].

$$\frac{\sigma_t}{f_t} = f(\omega) - \frac{\omega}{\omega_c} f(\omega_c) \tag{7}$$

$$f(\omega) = \left[1 + \left(\frac{c_1\omega}{\omega_c}\right)^3\right] e^{\left(-\frac{c_2\omega}{\omega_c}\right)} \tag{8}$$

$$G_f = 73 f_c^{0.18} \tag{9}$$

where ω = cracking displacement, ω_c = failure cracking displacement; and $\omega_c = 5.14 G_f/f_t$, $c_1 = 3.0$, $c_2 = 6.93$ for normal density concrete.

The stress–strain relationship of the structural and reinforcement steels used by Loh et al. [27] are employed and are plotted in Fig. 17(c) and (d), respectively. In these figures, f_{ys}, f_{us} and ε_{ys} are the yield stress, ultimate stress and yield strain of structural steel, respectively, and f_{yr}, f_{ur} and ε_{yr} are the yield stress, ultimate stress and yield strain of the reinforcement, respectively. The tension–separation relation proposed in Section 2.3.4 is used to define the nonlinear tension behavior of the connector element. Linear behavior is used for the shear–slip relation in the horizontal direction. Shear stiffness is computed using Eq. (10), which is proposed by the authors of this paper based on extensive experimental data and the theory of beams on elastic foundation [28].

$$k_s = 0.32 d_s E_s^{0.25} E_c^{0.75} \tag{10}$$

4.5. Verification of finite element model

For verification of the analytical model, mean values of the material properties obtained from the tests are used in the finite element analysis, and Fig. 18 compares the moment–separation curves derived from the finite element analysis and the tests. It can be seen that the ascending branches of the curves compare very well. Table 4 shows other more detailed comparisons. The maximum difference of the strength and stiffness between the simulations and tests are about 8% and 21%, respectively. In addition, readings of the eight displacement sensors attached to the top flange are also used to further verify the accuracy of the numerical simulations. Comparison of the relative separations between the concrete slab and top flange at the maximum moment obtained from the numerical simulations and tests is shown in Fig. 19. The simulation accurately captures the deformation of the top flange with a maximum discrepancy of 15%. Therefore, the developed finite element model is considered to be reliable and is employed to study the local behavior of the connections.

5. Numerical results of concrete slab-to-steel girder top flange connections

The experimental programs described in this paper evaluate the transfer of transverse moments in the bridge deck to steel bridge girders. Transverse moments develop in the bridge deck because of the geometry and load distribution, but very little transverse moment is transferred to the girder in most portions of the girder span, because the flexibility of the girder web permits limited rotation of the beam flange and avoids the restraint needed to develop moment transfer. Web stiffeners or other elements connected to

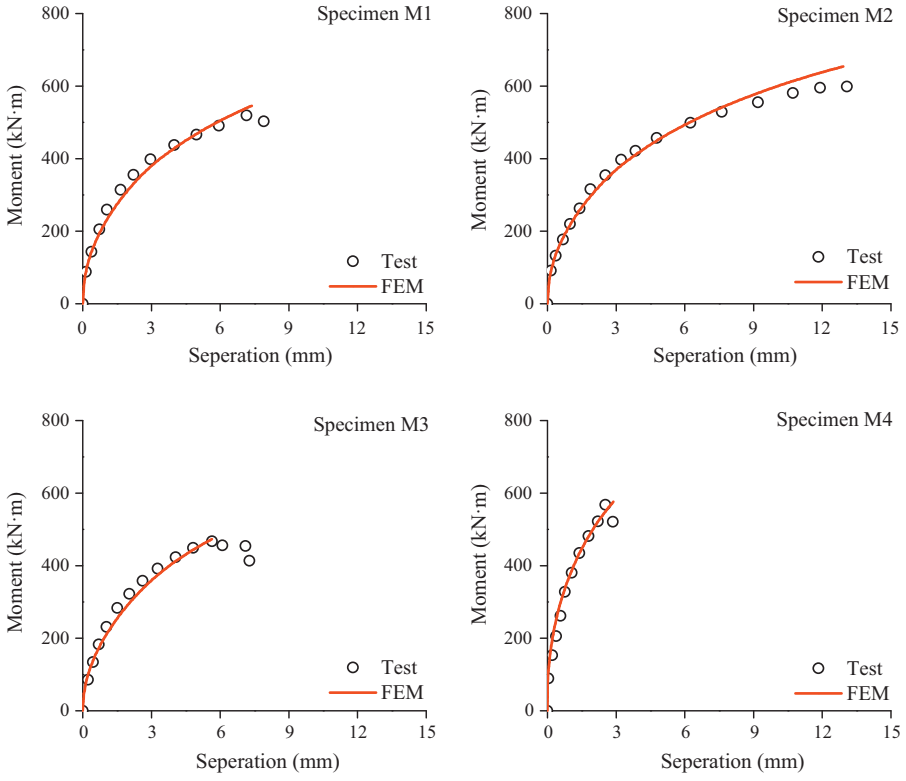

Fig. 18. Comparison of the moment–separation curves derived from the numerical simulations and tests.

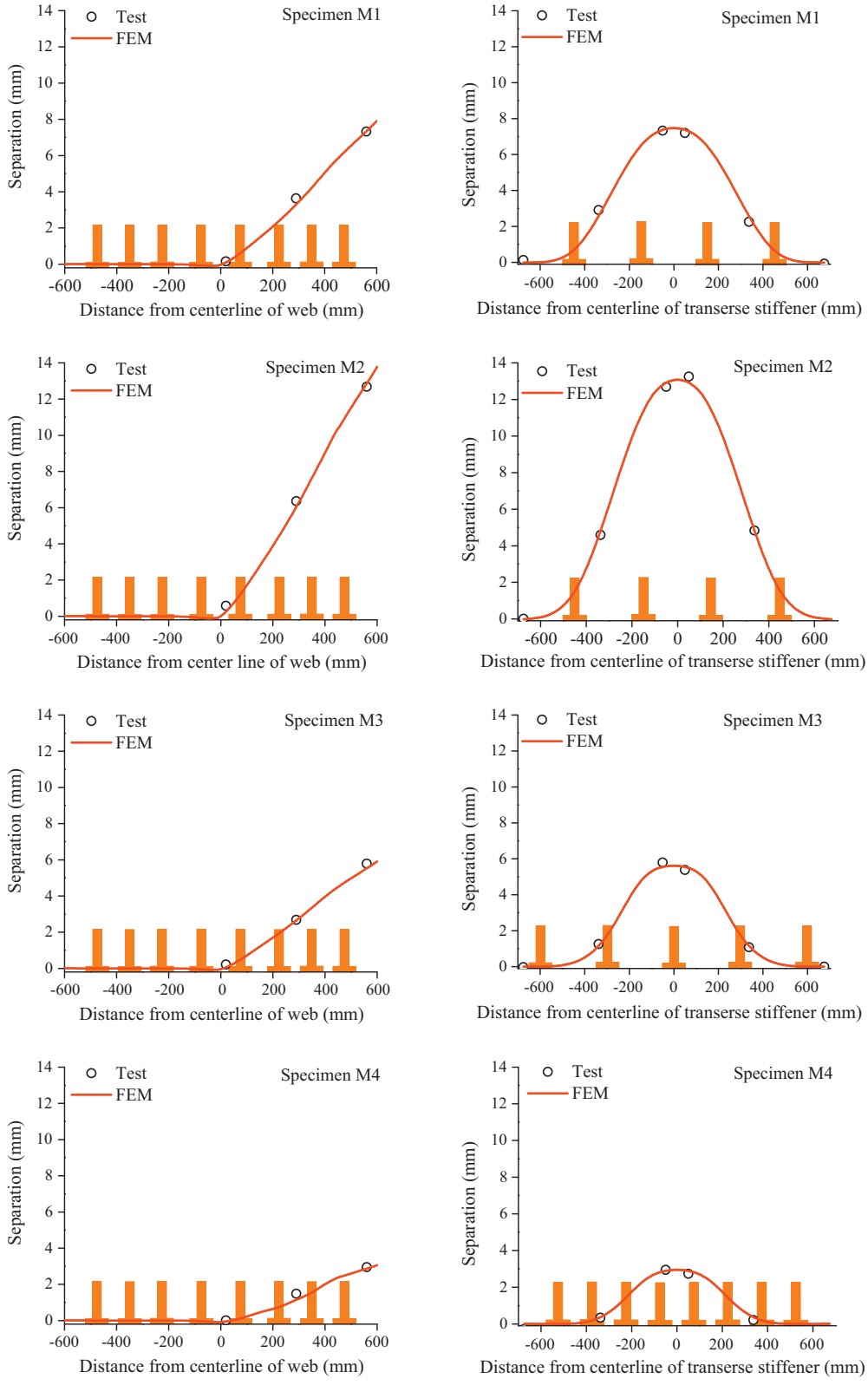

Fig. 19. Comparison between separations derived from numerical simulations and tests.

the flange increase the out-of-plane stiffness of the web and the rotational restraint of the flange in this local region. When this local restraint is present, significant local transverse moment transfer between the deck and the girder may occur. This transfer of the bending moment from the bridge deck to the steel girder will cause local compressive contact stress between the concrete deck and the flange and tensile force in stud connectors. Because of the local nature of this moment transfer, these stud forces may vary widely, and it is important to understand the distribution of compressive contact stress between the steel flange and the

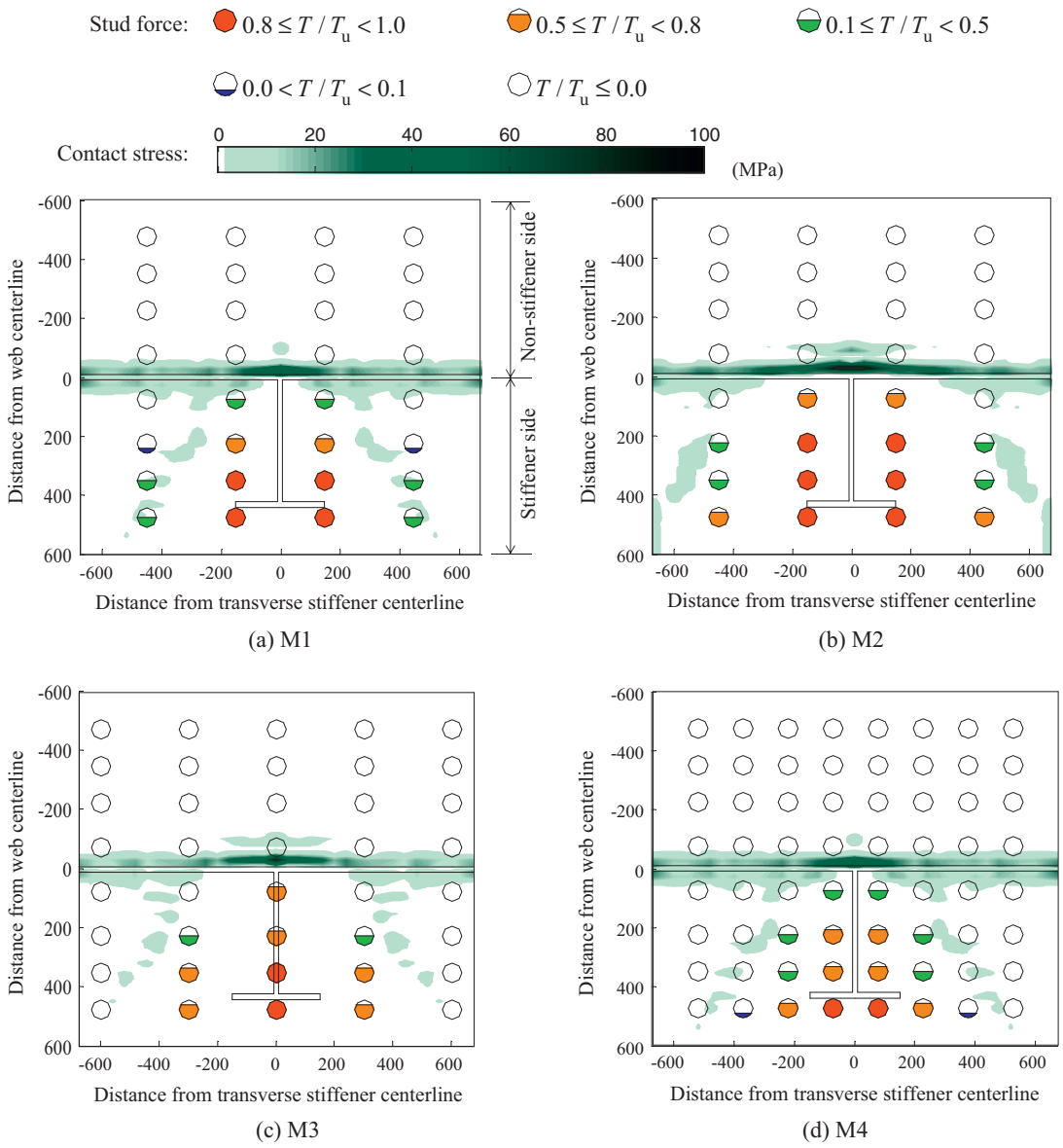

Fig. 20. Distribution of contact stress on the surface of the top flange and tension force in stud connectors.

concrete deck and the distribution of local tensile forces in the stud connectors. This information cannot be easily determined by experiments, and therefore, the verified analytical model is used to better understand this local variation and the parameters affecting this performance.

Fig. 20 presents the computed distribution of contact stress on the surface of the top flange at peak load and the distribution of tensile forces in the studs. The steel flange surface is transversely divided into two parts, as illustrated in Fig. 20(a). The half region having the transverse stiffener is defined as stiffener side, while the other half region is non-stiffener side. The value of contact stress is from 0 MPa to 100 MPa. For all specimens, large compressive contact stresses appear in the area within 50 mm of the steel web centerline on both stiffener and non-stiffener sides for all the specimens. Other compressive contact stress occurs in some area away from the steel web on the stiffener side. These appear analogous to prying forces noted in flexible bolted connections and are likely caused by the limited length and restraint in the test specimen.

The variation in axial force in the stud connectors is shown by circles with various colors. Four tension force to tension strength ratios are used to show the participation and contribution of each stud connector. A ratio exceeding 0.8 indicates that the stud has yielded. This is based on the fact that material test show that yield strength of a stud is about 80% of its ultimate strength. Based upon the results of pull-out tests, a ratio of approximately 0.5 shows where a stud connector enters the nonlinear separation phase. Shear–tension interaction of the stud can be ignored if tension force is less than 10% of the strength under pure tension [29], and so the 0.1 ratio is also included. Finally, the ratio of not greater than 0.0 is used to identify studs that are not in tension.

The computations show that studs on the non-stiffener side are either have a small tensile force or are in compression. Therefore, the effect of these studs is ignored. This shows that the studs on the stiffener side primarily contribute to the longitudinal bending moment resistance of the beam. Specimens M1 and M2 have two rows of studs on either side of the transverse stiffener, and both rows have studs in tension. For specimens M3 and M4, no stud

in the outmost row on either side of the transverse stiffener is under tension. One stud in the third row on either side of the transverse stiffener for specimen M4 is under tension.

For design of the stud connectors, it can be concluded that only the two innermost rows of studs on either side of the transverse stiffener participate in the bending moment transfer. For specimens M1 and M2, compressive contact occurs in the area between the outmost row of studs on either side of the transverse stiffener and the transverse edges of the top flange, and no stud would be under tension even if additional rows of studs were installed. Specimen M3 has studs installed directly over the web stiffener. This specimen attracts large tensile forces in that row of studs and only one row of stud connectors closest to the transverse stiffener on either side are under tension. Specimen M4 has closer stud spacing with studs straddling the web stiffener, and this causes more rows of studs to develop tensile force. This results in relatively large moment transfer but the peak capacity is achieve at small separation as shown in Fig. 15. One stud in the third row on either side of transverse stiffener is in tension, but the tension force in it is less than 10% of the tensile capacity and shear–tensile interaction may be neglected. Therefore, shear–tension interaction effect should be checked for the two innermost rows of studs on either side of the transverse stiffener in the design of a steel–concrete composite bridge.

In the longitudinal direction, the tensile force in the two rows of studs closest to the centerline of the transverse stiffener accounts for about 80%, 87%, and 65% of the total tensile force for specimens M1, M2, and M4, respectively. This indicates that as the distance between the second row of studs and the transverse stiffener reduces, the second row of studs contributes more to the moment resistance. Specimen M3 had a row studs directly over the stiffener, and the two adjacent rows contributed only about 50% of the total tensile force. In the transverse direction, the tensile force in a stud increases as its transverse distance from the steel web increases since the upward displacement is becoming larger with the increasing of the transverse distance. The pull-out tests show that a long stud connector needs to develop more separation than a short stud connector to resist the same tensile force. Therefore, varying stud heights in the transverse direction may result in a more uniform distribution of tension force in stud connectors on the stiffener side.

Based on the above conclusions, stud connectors with various heights are used at the interface between the concrete slab and top flanges in the steel–concrete composite bridges described and illustrated in Fig. 1. Because of the wide concrete cantilever and large live loads, 300 mm stud connectors are adopted in the outmost line on either side of the steel webs to increase the bending moment and deformation capacities of the stud connection at the interface, as shown in Fig. 21. In the region near transverse stiffeners, four lines of 300 mm stud connectors are used.

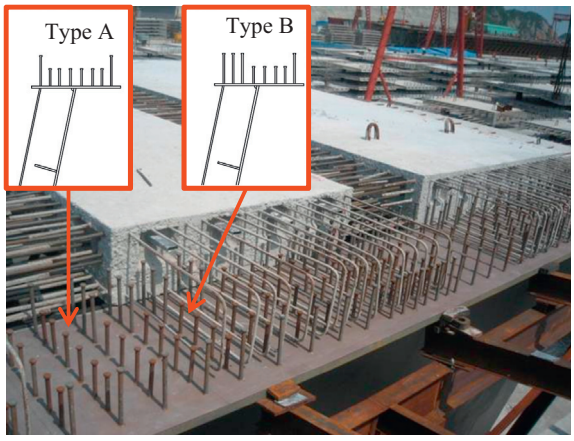

Fig. 21. Arrangement of stud connectors on the top flanges.

6. Conclusion

In this study, four groups of pull-out tests are performed to study the behavior of a single stud connector under tension force, and four connections with stud groups near transverse stiffeners are tested to investigate their global behavior under transverse bending moment. Numerical models of the four stud connections are developed to explore the local behavior at the interface. Based on the experimental and numerical studies, the following conclusions have been drawn:

(1) Stud height has a great influence on failure modes, tension strength and ultimate separation between the steel flange and concrete deck. The one group of pull-out specimens with a height–diameter ratio of 4.55 fails by cone pull-out of the concrete, while the other three groups of specimens with a minimum height–diameter ratio of 9.09, stud shank failure with larger tensile deformations are observed. The average strength of all the specimens failing due to stud shank fracture is 166.5 kN, which is about 1.53 times of the average strength of those failing due to concrete cone pull-out.
(2) For the pull-out specimens failing due to stud fracture, both the peak and ultimate separations increase as the stud height increases. A formula of peak separation and an expression of tension–separation relation, which considers the influence of peak separation, are developed from the test data. The proposed expression assumes that tension force in a stud connector reaches its maximum value at the peak separation, which is determined from the experimental results.
(3) The stud connection test results suggest that long stud connectors can effectively increase both the bending moment and deformation capacities of the connection. Reducing the longitudinal stud spacing significantly increases the stiffness. Stud connectors should not be welded directly over the transverse stiffeners, because the connection with this detail has reduced resistance and separation capacity.
(4) The numerical results show that compressive contact stress occurs mostly in the area within 50 mm from the centerline of the steel web and partly in some area away from the steel web due to the large local deformation of the top flange under the tension force of stud connectors.
(5) The stud connectors in the two innermost rows on either side of the transverse stiffener participate in resisting the tension force caused by the transverse bending moment transfer. Shear–tension interaction effect should be checked for these stud connectors in the design of a steel–concrete composite bridge. The tension force in a stud connector increases as its distance from the steel web increases and its distance from the transverse stiffener decreases.

References

[1] Collings D. Steel–concrete composite bridges: designing with eurocodes. 2nd ed. London: ICE Publishing; 2013.
[2] El-Lobody E, Lam D. Finite element analysis of steel–concrete composite girders. Adv Struct Eng 2003;6(4):267–81.
[3] Viest IM, Fountain RS, Singleton RC. Composite construction in steel and concrete for bridges and buildings. New York: McGraw-Hill; 1958.
[4] Johnson RP. Composite structures of steel and concrete. Oxford: Blackwell Scientific; 1994.

[5] Ollgaard JG, Slutter RG, Fisher JW. Shear strength of stud connectors in lightweight and normal-weight concrete. AISC Eng J 1971;8(2):55–64.
[6] Oehlers DJ, Coughlan CG. The shear stiffness of stud shear connections in composite beams. J Constr Steel Res 1986;6(4):273–84.
[7] Shim CS, Lee PG, Yoon TY. Static behavior of large stud shear connectors. Eng Struct 2004;26(12):1853–60.
[8] Lam D, El-Lobody E. Behavior of headed stud shear connectors in composite beam. J Struct Eng 2005;131(1):96–107.
[9] Badie SS, Morgan Girgis AF, Tadros MK, et al. Full-scale testing for composite slab/beam systems made with extended stud spacing. J Bridge Eng 2011;16 (5):653–61.
[10] Qureshi J, Lam D, Ye J. The influence of profiled sheeting thickness and shear connector's position on strength and ductility of headed shear connector. Eng Struct 2011;33(5):1643–56.
[11] Xue Dongyan, Liu Yuqing, Yu Zhen, et al. Static behavior of multi-stud shear connectors for steel–concrete composite bridge. J Constr Steel Res 2012;74:1–7.
[12] Guezouli S, Lachal A, Nguyen QH. Numerical investigation of internal force transfer mechanism in push-out tests. Eng Struct 2013;52:140–52.
[13] Chen L, Ranzi G, Jiang S, et al. An experimental study on the behaviour and design of shear connectors embedded in solid slabs at elevated temperatures. J Constr Steel Res 2015;106:57–66.
[14] Noel M, Wahab N, Soudki. Experimental investigation of connection details for precast deck panels on concrete girders in composite deck construction. Eng Struct 2016;106:15–24.
[15] Xu C, Sugiura K, Masuya H, et al. Experimental study on the biaxial loading effect on group stud shear connectors of steel–concrete composite bridges. J Bridge Eng 2015;20(10):04014109.
[16] Vayas I, Iliopoulos A. Design of steel–concrete composite bridges to eurocodes. Boca Raton: CRC Press; 2014.
[17] McMackin PJ, Slutter RG, Fisher JW. Headed steel anchor under combined loading. AISC Eng J 1973;10(2):43–55.
[18] Pallarés L, Hajjar JF. Headed steel stud anchors in composite structures, Part II-tension and interaction. NSEL report series: NSEL-014; 2009.
[19] Mirza O, Uy B. Effects of the combination of axial and shear loading on the behaviour of headed stud steel anchors. Eng Struct 2010;32(1):93–105.
[20] Professional Standard of the People's Republic of China. Code for design of highway reinforced concrete and prestressed concrete bridges and culverts, JTG D62-2004. Beijing: China Communication Press; 2004 (in Chinese).
[21] ACI 318-08. Building code requirements for structure concrete (ACI 318-08) and commentary (ACI 318R-08). MI: American Concrete Institute Farmington Hills; 2008.
[22] ABAQUS standard user's manual, version 6.10. USA: Hibbitt, Karlsson and Sorensen; 2010.
[23] Cook RA, Klingner RE. Behavior and design of ductile multiple anchor steel-to-concrete connections. Research rep. no. 1126-3; 1989.
[24] Carreira DJ, Chu KH. Stress–strain relationship for plain concrete in compression. ACI J Proc 1985;82(6).
[25] Cornelissen HAW, Hordijk DA, Reinhardt HW. Experimental determination of crack softening characteristics of normal weight and lightweight concrete. HERON 1986;31(2).
[26] FIB-Fédération Internationale du Béton. Model code 2010 (first complete draft), bulletin 55, vol. 1. Lausanne; 2010.
[27] Loh HY, Uy B, Bradford MA. The effects of partial shear connection in the hogging moment regions of composite beams Part II—analytical study. J Constr Steel Res 2004;60(6):921–62.
[28] Lin Z, Liu Y, He J. Research on calculation method of shear stiffness for headed stud connectors. Eng Mech 2014;31(7):85–90 (in Chinese).
[29] Lin Z, Liu Y, He J. Behavior of stud connectors under combined shear and tension loads. Eng Struct 2014;81:362–76.